
Article:
Di Lauro, M., Casalini, S., Berto, M. et al. (6 more authors) (2016) The Substrate is a pH-Controlled Second Gate of Electrolyte-Gated Organic Field-Effect Transistor. ACS Applied Materials and Interfaces, 8 (46). pp. 31783-31790. ISSN 1944-8252

https://doi.org/10.1021/acsami.6b06952

ACS APPLIED MATERIALS & INTERFACES

Article

The Substrate is a pH-Controlled Second Gate of Electrolyte-Gated Organic Field-Effect Transistor

Michele Di Lauro, Stefano Casalini, Marcello Berto, Alessandra Campana, Tobias Cramer, Mauro Murgia, Mark Geoghegan, Carlo Augusto Bortolotti, and Fabio Biscarini

ACS Appl. Mater. Interfaces, **Just Accepted Manuscript** • DOI: 10.1021/acsami.6b06952 • Publication Date (Web): 22 Sep 2016

Just Accepted

ACS Publications

ACS Applied Materials & Interfaces is published by the American Chemical Society.
1155 Sixteenth Street N.W., Washington, DC 20036

The Substrate is a pH-Controlled Second Gate of Electrolyte-Gated Organic Field-Effect Transistor

Michele Di Lauro[1], Stefano Casalini[1], Marcello Berto[1], Alessandra Campana[2], Tobias Cramer[3], Mauro Murgia[2], Mark Geoghegan[1,4], Carlo A. Bortolotti[1,5], Fabio Biscarini[1*]

[1]Dipartimento di Scienze della Vita, Università di Modena e Reggio Emilia, Via G. Campi 103, 41125 Modena, Italy

[2]Consiglio Nazionale delle Ricerche, Istituto per lo Studio dei Materiali Nanostrutturati (CNR-ISMN), Via P. Gobetti 101, 40129 Bologna, Italy

[3]Dipartimento di Fisica e Astronomia, Alma Mater Studiorum-Università degli Studi di Bologna, V.le Berti-Pichat 6/2, 40127 Bologna, Italy

[4]Department of Physics and Astronomy, University of Sheffield, Hounsfield Road, Sheffield S3 7RH, UK

[5]Consiglio Nazionale delle Ricerche, CNR-NANO Via Campi 213/a, 41125 Modena, Italy

KEYWORDS Pentacene; EGOFET; capacitive coupling; biosensors; bioelectronics.

ABSTRACT: Electrolyte-gated organic field-effect transistors (EGOFETs), based on ultra-thin pentacene films on quartz, were operated with electrolyte solutions whose pH was systematically changed. Transistor parameters exhibit non-monotonic variation vs pH, which cannot be accounted for by capacitive coupling through the Debye-Helmholtz layer. The data were fitted with an analytical model of the accumulated charge in the EGOFET where Langmuir adsorption was introduced to describe the (pH-dependent) charge build-up at the quartz surface. The model provides an excellent fit to the threshold voltage and transfer characteristics as a function of pH, which demonstrates that quartz acts as a second gate controlled by pH, and is mostly effective at neutral or alkaline pH. The effective capacitance of the device is always greater than the capacitance of the electrolyte, thus highlighting the role of the substrate as an important active element for amplification of the transistor response.

INTRODUCTION

Since the pioneering work of Bergveld[1] several examples of field-effect transistors (FETs) have been demonstrated as sensors working in aqueous solutions.[2] In the ion-sensing field-effect transistor (ISFET), a reference electrode controls the potential of an electrolyte solution at the interface with a metal-oxide-semiconductor FET (MOSFET). The ISFET is a potentiometric sensor that responds to the activity of ions, in particular hydronium ions, at the electrolyte/dielectric/semiconductor interface. Ion-sensitive organic field-effect transistors (ISOFETs) were also demonstrated, where the channel consists of an organic semiconductor (OSC) thin film.[3,4] In these architectures, an encapsulation layer separating the organic semiconductor thin film from the aqueous environment has been used. Both inorganic (*e.g.* silicon nitride[3] and tantalum pentoxide[4]) and organic (*e.g.* poly(methyl methacrylate)[5] and poly(vinylidene fluoride))[6] dielectrics were exploited to yield pH-sensitive devices.

It is also possible to operate the IS(O)FET in a dual gate architecture, where the bottom gate consists of a metal electrode separated by a (bottom) dielectric, and the top gate electrode controls the bath potential. The two gates are operated independently, giving rise to a dual channel in a thick film (if the signs of gate voltages are the same) or depleting one of the channels (if their signs are opposite). It was shown[7,8] that the device responds with a shift of threshold voltage to changes of the top-gate potential. The shift observed is proportional to (the negative of) the potential change at the top gate, through a capacitive coupling given by the ratio of the top and bottom capacitances. Because the two capacitances can be independently controlled by choice of material (relative permittivity) and dielectric film thickness, the capacitive coupling can be made greater than 1, thus amplifying the top gate voltage.

Recently, water-stable devices operated in solution without the top dielectric layer were demonstrated.[9] They were termed electrolyte-gated organic field-effect transistors (EGOFETs).[10] The absence of the top dielectric layer not only makes the processing easier, but it also endows the device with greater sensitivity due to the direct contact between the electrolyte and the conductive channel.[11] Several architectures of pH-sensitive EGOFETs were demonstrated.[12,13] Thin film transistors with α-sexithienyl exhibit a response to local pH-changes at the channel surface with a sensitivity of 9 mV per pH unit.[13] In another architecture, an ion-selective membrane separates the electrolyte in two aqueous compartments: the first one (in direct contact with the organic semiconductor) is filled with a phosphate buffer solution while the second (where pH changes are occurring) is in contact with the gate electrode.[12] EGOFETs are capable of detecting biologically-relevant phenomena, such as enzymatic[14] and chemical reactions,[15] DNA hybridization,[16] immunorecognition,[17] local pH-changes[13] and bioelectric signals.[18] The ultra-high sensitivity[19] and selectivity to individual analytes make the EGOFET a promising candidate for biomedical applications.

The exact mechanism and the origin of the sensitivity in EGOFET devices are not understood. When an EGOFET was operated as a dual gate OFET with a bottom silicon oxide dielectric, a capacitive coupling in aqueous electrolytes up to

1000 times was observed.[11] This hints at an explanation of why EGOFETs transduce extracellular potential changes as small as a few tens of μV from the activity of neuronal cells into tens of mV threshold voltage shift.[20]

An understanding of the large capacitive coupling of EGOFETs is more elusive when only the liquid gate is accounted for. In EGOFETs built on a solid substrate or polymeric scaffold, the role of the substrate is either neglected or the substrate is treated as a passive element of the device that manifests a floating potential. The hypothesis addressed here is that the substrate surface, in conjunction with the electrolyte, gates the organic semiconductor film, thus substantially contributing to the accumulation of charge carriers in the channel.

To prove this, quartz, whose surface charge is pH-dependent, is used as the substrate in the fabrication of pentacene EGOFETs. Quartz is amphoteric because of the presence of silanol groups at the surface. The quartz surface is positively charged at pH < ~3; increasing the pH above the point of zero charge leads to deprotonation of the silanols that results in a negative surface charge. EGOFETs were characterized upon systematically changing pH from 3 to 10. The observed non-monotonic EGOFET response to pH is explained here by means of the capacitive coupling of the substrate through its surface chemistry. In this scenario, the organic semiconductor thin film does not isolate the substrate surface from the electrolyte. The coupling of a bare dielectric surface (as in ISFETs) to the electrolyte is usually described by the site-binding model[21] where the ion-activity determines the surface potential. The site-binding model strictly applies to 1:1 electrolytes, whereas many relevant EGOFETs operate in physiological solutions (either phosphate buffer or cell-culture medium). To overcome these limitations, a model integrating the Langmuir isotherm of acidic dissociation of the quartz surface and the Debye-Helmholtz theory of surface/electrolyte interfaces has been devised. Our model describes the substrate contribution to the build-up of charge in the organic semiconductor. It fits the whole pH-dependence of the transfer characteristics and predicts the capacitive coupling of the EGOFET. The EGOFET effective capacitance exceeds the capacitance of the electrolyte double layer by between two and ten.

RESULTS AND DISCUSSION

The device layout is schematically depicted in Fig. 1a. The pentacene film forms the channel between source and drain electrodes patterned on quartz substrate. The gate electrode controls the electrochemical potential of the electrolyte confined within polypropylene (PP) walls.

For each pH from 3 to 10 in steps of one pH unit, the transfer characteristics I_{DS} vs. V_{GS} were recorded in the saturation regime (*i.e.* V_{DS} = –400 mV, –400 mV < V_{GS} < 200mV) described by

$$I_{DS} = \frac{W}{2L}\mu C_{eff}(V_{GS} - V_{th})^2. \quad (1)$$

Here I_{DS} is the source-drain current, W and L are channel width and length respectively, C_{eff} is the effective capacitance per unit area between semiconductor and gate, μ is the charge carrier mobility, V_{GS} is the gate-source voltage and V_{th} is the threshold voltage. The V_{th} values were extracted by the linear fit of the experimental $I_{DS}^{1/2}$ *vs* V_{GS} data for –400 mV< V_{GS} < –350 mV.

Fig. 1b shows the EGOFET response at pH = 7. The threshold voltage is V_{th} = +33 mV and the ON-current is as high as 3.37 μA, in line with standard values in EGOFETs.

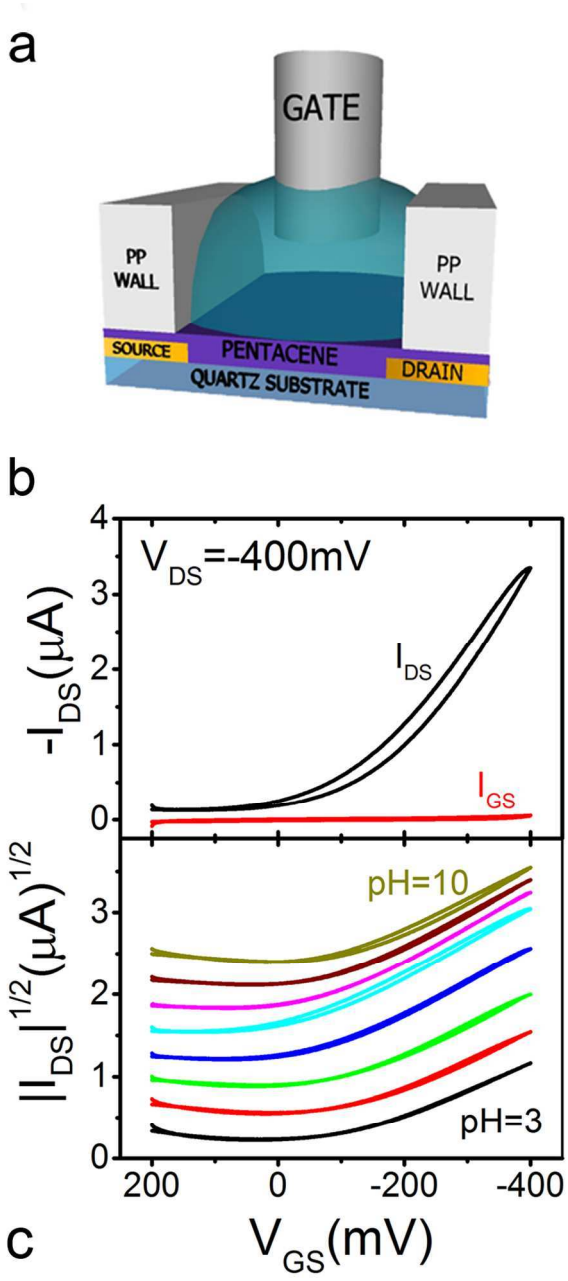

FIGURE 1. a) Schematic layout of the EGOFET device on quartz; b) Transfer characteristic in saturation regime (black) and leakage source-gate current (red), recorded at V_{DS}= -400mV and pH = 7); c) Evolution of the transfer characteristics in response to electrolyte pH changes (each curve has been vertically offset in increments of 0.33 $\mu A^{1/2}$ for clarity).

The modest hysteresis of the characteristics is typical for such devices, and the leakage current is tens of nA. It can be inferred that no electrochemical doping occurred in these devices.[9]

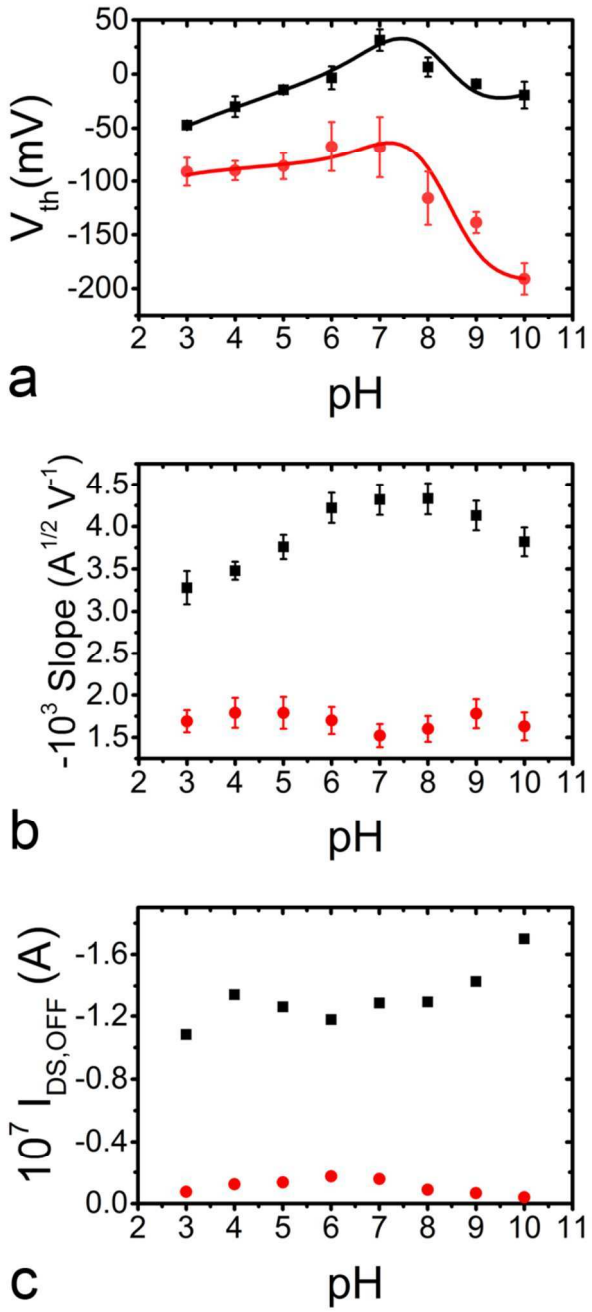

FIGURE 2. pH dependence of EGOFET characteristics for bare (black squares) and HMDS-passivated (red dots) devices: a) Threshold voltage (solid lines are fits according to the model given by eq 10); b) Slope of the linear region of the $I_{DS}^{1/2}$ vs. V_G plots; c) Off-current (error bars are comparable to marker's size).

To assess both the stability of the device and the reversibility of the pH response, the pH of the electrolyte solution was systematically changed from pH 3 to 10. Checks were also made to demonstrate that the variation was independent of the direction of the pH change and it was concluded that there was no hysteresis in these measurements. Fig. 1c shows typical variations of the transfer characteristics upon increasing the pH of the electrolyte. Upon pH modulation a shift of the threshold voltage and a change of the slope of the transfer characteristics can be observed. This evidence suggests a pH-dependent interplay between changes in carrier density within the OSC and the evolution of capacitance (which is proportional to the slope of the transfer curve).

To demonstrate the role of substrate charge on EGOFET behavior, a further batch of EGOFETs was fabricated with the quartz exposed to hexa-methyl-di-silazane (HMDS) prior to pentacene deposition. This surface treatment decreases the density of free silanols because of the condensation of 3-methylsylanol from HMDS.

Fig. 2a shows the comparison of the extracted V_{th} values for bare quartz and HMDS-functionalized devices as a function of electrolyte pH. The devices on bare quartz (black squares) exhibit a non-monotonic V_{th} dependence on pH, with a peak around pH = 7. The values of V_{th} are mostly negative away from pH = 7, suggesting that trap states with a higher energy (more negative voltage) are created for holes in pentacene both at low and high pH. The slopes of V_{th} vs. pH are similar both under acidic and alkaline conditions, with a value approximately equal to 20 mV per pH unit. The linear slopes of (saturation) transfer characteristics of bare-quartz devices vs. pH (Fig. 2b) also exhibit a maximum at pH = 7. The (absolute) off-current, on the other hand, increases with pH (Fig. 2c) as a consequence of the increased carrier density induced by the quartz surface charge.

Referring now to the device with the passivated substrate (red dots), the threshold voltage is pH independent in the acidic range, while in the alkaline range V_{th} monotonically decays with increasing pH. It is noted that V_{th} is always negative, in contrast to that of bare quartz. Neither the slope (Fig. 2b) nor the off-current (Fig. 2c) extracted from the transfer characteristics of the HMDS-passivated devices exhibits significant pH dependence.

A quantitative description of the non-monotonic experimental behavior shown in Fig.s 2a and b is provided by means of the model depicted in Fig. 3a. Next, an analytical expression for the charge in the pentacene film will be developed thus accounting for the pH-dependent variations of V_{th}. In the model an intrinsic effective charge Q_{int} is present in the OSC to account for dopants, trap states and film defects. The rest of the charge in pentacene is expressed as the sum of two terms: one, $-Q_q$, is an image charge of the negative surface charge contributed by the dissociated silanol groups; the other, $-Q_2$, is accumulated because of the capacitance $A_{ch}C_2$ at the interface between the OSC and the electrolyte, where $A_{ch}= WL$ is the channel area. The total charge Q_{P5} accumulated in pentacene can therefore be expressed as:

$$Q_{P5} = Q_{int} - Q_q - Q_2. \quad (2).$$

If the charge in the capacitor C_1 at the gate/electrolyte interface is denoted Q_1, the electroneutrality of the electrolyte solution imposes $Q_2 = -Q_1$. Therefore, eq 2 is recast as:

$$Q_{P5} = Q_{int} - Q_q + Q_1. \quad (3).$$

It is necessary at this point to obtain analytical expressions for the pH dependence of Q_1 and Q_q, so that they can be substituted into eq 3. First, the gate/electrolyte interface is considered, by expressing the pH dependence of Q_1 using Debye-Helmholtz theory. The Debye screening length λ_D of the electric field is expressed as a function of the ionic composition of the electrolyte,

$$\lambda_D = \sqrt{\frac{\varepsilon\varepsilon_0 k_B T}{q^2 \sum_{m=1}^{N_{ion}} z_m^2 c_m}}, \quad (4)$$

where ε, ε_0, k_B and T are the relative permittivity of the electrolyte, the vacuum permittivity, the Boltzmann constant, and the absolute temperature, respectively; q is the elementary charge and z_m and c_m are the number charge and number concentration [m^{-3}] of the m-th ion. Since the exact ionic composition of the electrolyte at any pH can be calculated from the acid dissociation constants of phosphoric acid in water ($pK_{a,1}$, $pK_{a,2}$ and $pK_{a,3}$ whose values are 2.14, 7.10 and 12.40, respectively), λ_D is obtained from eq 4, and inserted into the expression for the areal capacitance C_1 to give

$$C_1 = \frac{\varepsilon\varepsilon_0}{\lambda_D} = \sqrt{\frac{\varepsilon\varepsilon_0 q^2 \sum_{m=1}^{N_{ion}} z_m^2 c_m(\mathrm{pH})}{k_B T}}. \quad (5).$$

From eq 5, C_1 can be estimated at any pH if ε is constant. Based on previous investigations on the effect of ionic concentration on the dielectric constant of aqueous solutions,[22] the variation of ε, in the experimental conditions of the present work, would be on the order of 1.25%, and hence the values from eq 5 will be affected by no more than 1.12%. Fig. 3b shows the plot of the calculated Debye length and C_1 as a function of pH. Over the pH range investigated, λ_D decreases by about a third with increasing pH, resulting in roughly 50% increase of C_1.

The charge induced through the electrolyte capacitance C_1 is

$$Q_1 = (\Psi_B - V_G) A_G C_1(\mathrm{pH}), \quad (6)$$

is a function of the electrolyte bulk potential Ψ_B, the gate potential V_G and the gate area A_G.

Next the pH-dependent charge on the quartz surface is considered by treating surface titration within a Langmuir adsorption-type approach.[23] If N_S is the areal number density of amphoteric sites, and θ is the fraction of N_S that is deprotonated to silanoates, then

$$\theta = \frac{[OH^-]}{K_a + [OH^-]} = \frac{10^{pH}}{10^{14} K_a + 10^{pH}}, \quad (7)$$

where K_a = 1.8 10^{-6} is the acid dissociation constant of silanol.[24,25]

The number of deprotonated sites is proportional to the quartz surface charge:

$$Q_q = -A_{ch} q N_s \frac{10^{\mathrm{pH}}}{10^{14} K_a + 10^{\mathrm{pH}}} \quad (8)$$

By combining eqs 3, 6, and 8 the pH dependent expression for Q_{P5} is obtained:

$$Q_{P5} = Q_{int} + A_{ch} q N_s \frac{10^{\mathrm{pH}}}{10^{14} K_a + 10^{\mathrm{pH}}} + (\alpha\ \mathrm{pH} - V_G) A_G C_1. \quad (9)$$

In eq 9, following van Hal et al.,[26] a linear dependence of Ψ_B on pH (in our observed range) is assumed through the coefficient α.

The total charge Q_{P5}, as well as the charge contributed by the quartz surface Q_q and the capacitive charge Q_1 are shown in Fig. 3c for V_G = –400 mV. The curves are calculated with the best-fit parameters from Fig. 2a, as explained below. Close to pH = 7 there is a large (~50%) increase of the total accumulated

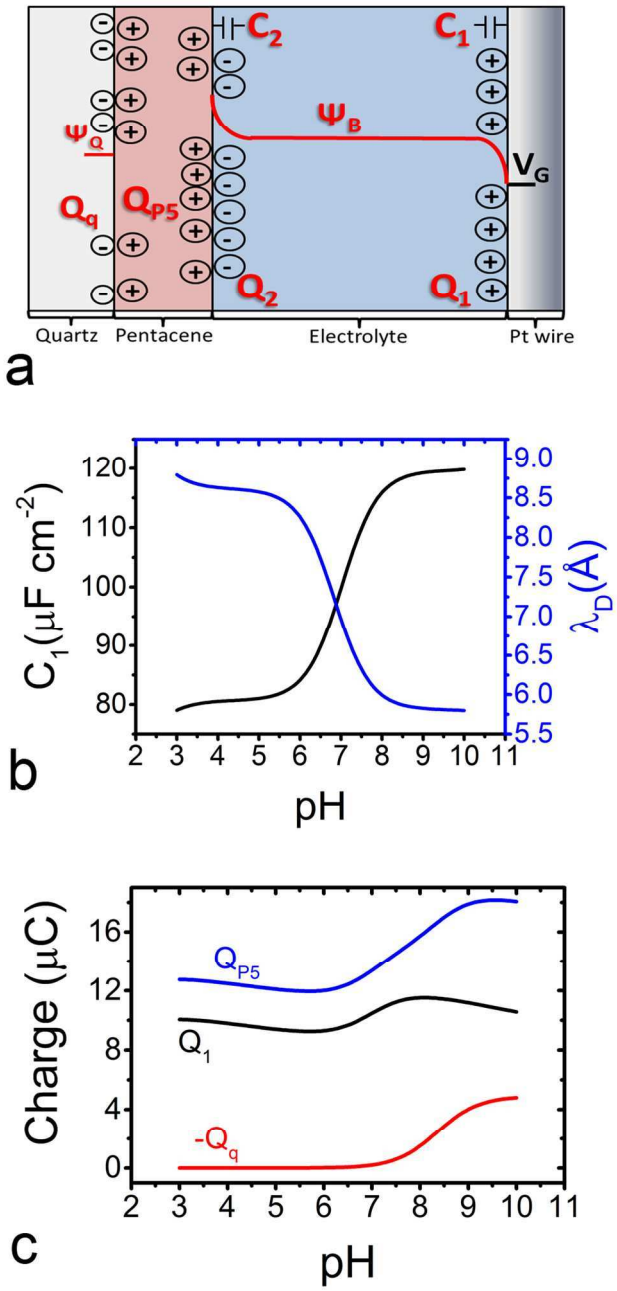

FIGURE 3. a) Schematic cross-section of the electrostatic model used to describe the V_{th} trend, pH-dependent quantities are highlighted in red; b) λ_D and C_1, calculated as a function of pH using eqs 4 and 5, respectively, for the electrolyte used in the present work; c) Plot of the calculated Q_1, $-Q_q$ and Q_{P5} vs. pH.

charge in pentacene Q_{P5}, due to the increase of both Q_1 (because of the increase of C_1) and Q_q (because of the complete deprotonation at high pH). The $-Q_q$ vs. pH trend (Fig. 3c) resembles that of the off-current of the bare quartz device (Fig. 2c). When measuring the off-current, the field-effect of the gate electrode is negligible. The modulation of the current is left only to the quartz surface whose charge is controlled by pH. Hence, for absolute gate voltages much lower than threshold voltage there is only one gate, and that is the quartz surface. It should be however noted that the off-current contains a

significant contribution from the leakage current, I_{GS}. A thorough treatment of the off-current and its deconvolution into its constitutive components will be reported elsewhere.

The pH dependence of the threshold voltage (Fig. 2a) can be explained by fitting the data with the electrostatic model above. Here V_{th} can be treated as the (negative of) V_G value that marks the onset of accumulation of positive charge in the channel (for a p-type semiconductor such as pentacene). Therefore, at $V_G = -V_{th}$, the total charge in the pentacene is zero. The V_{th} values in Fig. 2a can thus be fitted by

$$V_{th}(\mathrm{pH}) = \frac{-Q_{int}}{A_G C_1(\mathrm{pH})} - \left[\frac{A_{ch} q N_s}{A_G C_1(\mathrm{pH})}\right] \frac{10^{\mathrm{pH}}}{10^{14} K_a + 10^{\mathrm{pH}}} - \alpha\ \mathrm{pH} \quad (10)$$

The threshold voltage therefore comprises three terms dependent on pH. They relate to (from left to right in eq 10) the intrinsic charge of pentacene, the quartz surface and the electrolyte bath. The first contribution is proportional to the inverse capacitance and becomes less negative at higher pH. The second term, also negative and due to quartz, decreases from about zero to more negative values at high pH. The third term, linear in pH, is positive when $\alpha < 0$.

The best-fit curve on bare quartz is shown as the solid black line in Fig. 2a. It reveals the excellent agreement with the experimental data. The behavior of the device on bare quartz is reproduced by the parameters $N_S = 1.02 \pm 0.11\ 10^{16}$ cm^{-2}, $Q_{int} = 2.69 \pm 0.24$ μC and $\alpha = -15.5 \pm 1.7$ mV. The value of Ns is in agreement with other models;[26,27] if the channel area is $A_{ch} = 3.02\ 10^{-3}$ cm^2 and the thickness of pentacene is 15 nm, Q_{int} corresponds to a maximum density of dopants (each deprotonated site yields a charge in pentacene) of approximately $4\ 10^{20}$ cm^{-3}, *i.e.* 4 charges per 14 unit cells.[28] This is a high intrinsic doping level, about 3-6 orders of magnitude larger than that observed for pentacene transistors in ambient or in vacuum. The increase in V_{th} at low pH is mainly due to the third term (linear in pH) in eq 10. The peak of the threshold voltage around neutrality arises from the rapid change of the quartz surface potential (due to the deprotonation to silanoate as the pH approaches the pK_a), and from the steep increase of C_1 that also occurs approximately in the same pH region (around the $pK_{a,2}$ of the phosphoric acid). In brief, this simple model shows that the presence of the pH-sensitive substrate, and to some extent also the presence of charge in the OSC due to its intrinsic doping, introduce important deviations from the expected Nernst-like behavior.[8]

The model can be readily adapted to any electrolyte composition and first order surface-potential-determining process. Thus it can be applied to the V_{th} trend for the HMDS-passivated device (solid red line in Fig. 2a). Best-fit parameters are $N_S = 1.44 \pm 0.15\ 10^{16}$ cm^{-2}, $Q_{int} = 2.99 \pm 0.28$ μC and $\alpha = -3.66 \pm 2.0$ mV. The different surface chemistry appears in the smaller (in magnitude) value of α. Once again, the decay of V_{th} in the alkaline region is due to the large variation with pH of the substrate surface charge around pH = 7, which is much more substantial than the contribution due to the intrinsic charge divided by the capacitance C_1. Noticeably, the intrinsic charge and the density of sites undergoing deprotonation exhibit similar values to the ones observed with the bare quartz surface. While the former is possible due to the use of the same pristine material and to growth conditions, the latter is less obvious, as the functionalization with HMDS, which leads to condensation of the tri-methyl siloxane group on silanol, should result in a decrease of Ns. The observation that Ns is approximately the same as that of the bare quartz devices, may imply that the silanol groups on the HMDS-passivated devices are decapped at higher pH because of the onset of hydrolysis.[29] This does not occur at low pH, as reflected by the small α value.

Finally, the nature of the capacitive coupling between the gate electrode and the semiconductor channel is addressed. The effective capacitance C_{eff} of the EGOFET is defined as

$$C_{eff} = \frac{Q_{P5}(\mathrm{pH}, V_G)}{A_G |V_G|}, \quad (11)$$

where C_{eff} accounts for the total charge in the OSC. It depends not only on pH as would be expected, but also on V_G as shown in Fig. 4a. At a given pH, C_{eff} decreases as (the absolute value of) V_G increases. This decrease is mainly ascribed to the first two terms in eq 9 that do not depend on V_G, mainly the intrinsic charge and the quartz surface charge. The decrease in C_{eff} with pH is steeper at high pH than at low pH. Close to neutrality, however, the trend is reverted and C_{eff} increases at larger V_G.

Keeping V_G constant, the largest slope of C_{eff} vs. pH is observed at pH ≥ 7 and so at close to neutral pH the sensitivity to pH would be the highest. There, the effective capacitance undergoes a variation vs. pH of several tens of μC/cm^2 per pH unit at any gate voltage. There is also lower sensitivity at acidic pH. The effective capacitance, however, saturates at high pH. By considering the trend of C_{eff} vs. V_G at a given pH, it is clear that the strongest coupling is achieved at pH ≥ 7, when both the quartz surface charge and the electrolyte capacitance C_1 increase then saturate at large values. Thus, the substrate through its surface chemistry plays a primary role in the coupling between gate and channel.

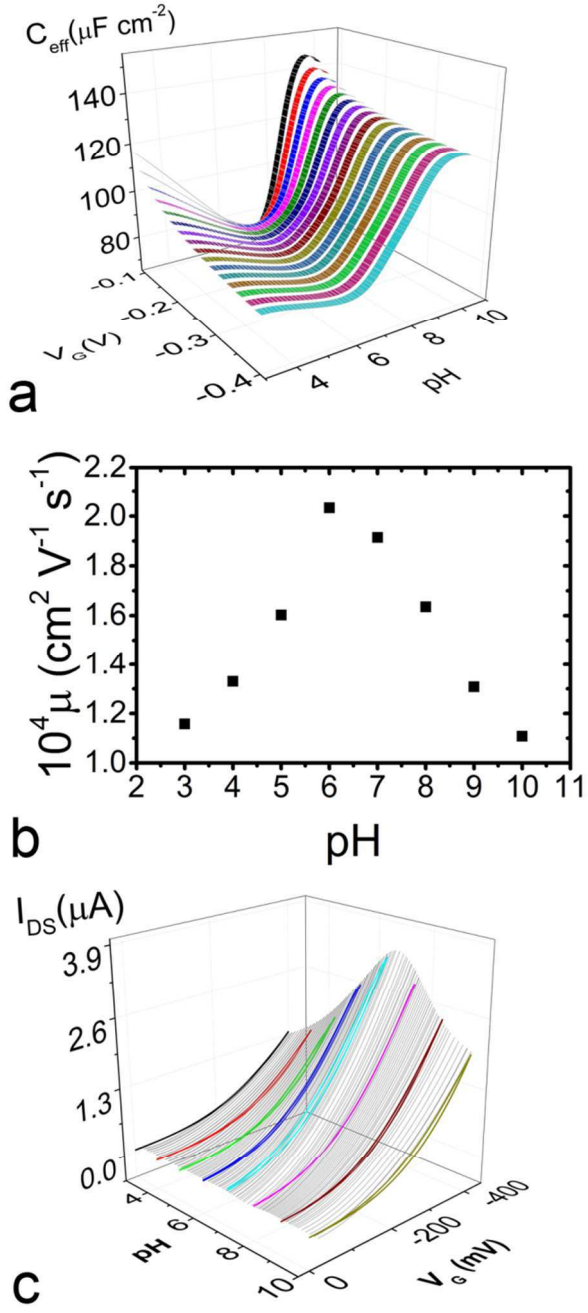

FIGURE 4. a) Dependence of C_{eff} on pH and V_G; b) Apparent mobility vs. pH (error bars are obscured by the data); c) Overlay of simulated transfer characteristics (black thin lines) with the experimental curves from Fig. 1b. The calculated curves were simulated using eq 1, with V_{th} obtained from the fit and using C_{eff} as capacitance.

Some general consideration related to EGOFET transducers can be provided. In a medium with buffer at pH = 7 a modulation of V_G or a modulation of pH, will induce a substantial change in the effective capacitance. For instance, any event (such as the adsorption of a molecular species, a voltage pulse applied to the gate electrode or a local change of pH) that shifts V_G to larger (smaller) absolute values will produce a decrease (increase) in the effective capacitance and hence a decrease (increase) in the slope of the transfer characteristics and in the current intensity. This hints at an explanation of the response observed in EGOFET biosensors: a biological event modulating the gate voltage will couple to the channel through a radically different C_{eff}.

Once the effective capacitance has been evaluated, the field effect mobility can be extracted from the slope of the $I_{DS}^{1/2}$ vs. V_{GS} plots (Fig. 2b) according to eq 1. The apparent charge mobility (Fig. 4b) exhibits a maximum at around pH = 7, where the effective capacitance has a minimum as a function of pH. It is emphasized that, because of the dependence of C_{eff} on V_G and pH (Fig. 4a), the charge mobility cannot be determined as an intrinsic material property, since it will inevitably reflect the pH-dependent behavior of C_{eff}. Based on the values extracted from fitting, the transfer characteristics can then be simulated as a function of pH. Fig. 4c shows a plot of the calculated transfer characteristics and the experimental curves reported in Fig. 1b. The characteristics that exhibit a larger variation are the ones in the proximity of pH = 7.

The importance of C_{eff} in understanding EGOFET performance is evident when comparing C_{eff} with the capacitance C_{eq} that arises from the in-series capacitances C_1 and C_2:

$$\frac{C_{eff}}{C_{eq}} = A_G C_{eff}\left(\frac{1}{A_G C_1} + \frac{1}{A_{ch} C_2}\right). \quad (12).$$

The ratio C_{eff}/C_{eq} is the capacitive coupling of the EGOFET and is shown as a function of pH in Fig. 5.

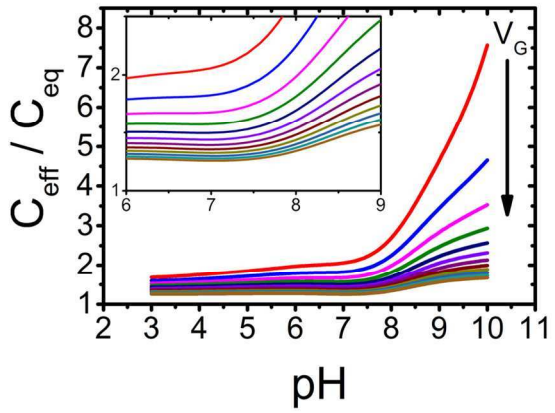

FIGURE 5. Ratio C_{eff}/C_{eq} as a function of pH for increasing $|V_G|$ (0.1 V < $|V_G|$ < 0.4 V) from top to bottom. The inset is a magnification of the 6 < pH < 9 range.

Noticeably, $C_{eff}/C_{eq} > 1$ for all pH and V_G measured. In particular, it rapidly increases at high pH and smaller $|V_G|$ almost an order of magnitude. Importantly, the slopes of the C_{eff}/C_{eq} curves in Fig. 5 show that the sensitivity is less in acidic environments and greater in the high pH region, with the sensitivity starting to increase at around neutrality. Smaller-in-magnitude gate voltages, *i.e.* within the sub-threshold region of the transfer curve, yield the largest sensitivities. One can estimate a gradient of at least 3 per pH unit at pH > 7 for the red curve (V_G = -100 mV) in Fig. 5. This response is related to the rapid rise in C_{eff} (Fig. 4a) over the same pH region (before C_{eff} attains a constant value at high pH).

This work demonstrates that in EGOFETs there is amplification, similarly to what happens in dual gate OFETs or ISFETs, where the interfacial potential is amplified by the ratio of top and bottom capacitances. Importantly, C_{eq} alone underestimates the charge accumulation in the organic semiconductor

in response to gate bias, because it ignores the contribution of the substrate surface. Despite of the coating by the organic semiconductor thin film, the substrate surface is not an insolated element of the device, instead it is accessible and chemically coupled to the electrolyte. This evidence is supported by atomic-force-microscopy investigation of the pentacene thin-film (see Fig. S3 in the Supporting Information) The modulation of the surface charge by the electrolyte is substantial and this is reflected on the coupling between the gate and the channel as well as the sensitivity as a function both of pH and V_G.

CONCLUSIONS

Pentacene EGOFETs on quartz have been systematically studied as a function of electrolyte pH. The pH dependence of the threshold voltage has been explained by accounting for the pH dependence of the surface charge of the quartz substrate and the composition of the electrolyte solution. The hypothesis that the substrate charge modulates EGOFET behavior was confirmed by control experiments using acid-insensitive devices with HMDS-passivated quartz surface. The experimental results were fitted to a model that provides a conceptually simple analytical expression relating the total charge in the OSC to electrolyte composition, pH and gate voltage.

When designing EGOFET devices, it is therefore important to consider the substrate as an active component of the device. The observed coupling of the substrate with the electrolyte environment is consistent with the operations of biosensors where the recognition moiety is grafted on the substrate and embedded under the semiconductor thin film.[30] In that case, the analyte (biotin) is even much larger than hydronium ions that are relevant to our study. The substrate therefore acts as a second auxiliary gate in the EGOFET architecture, as it induces a much stronger capacitive coupling with respect to the hitherto accepted scenario governed solely by the electrolyte. For a full understanding of the EGOFET response, one has to take into account both the substrate charge and the ionic composition of the electrolyte at the desired operational pH. This understanding of the effective device capacitance will enable the design and correct interpretation of the response of biosensors and cell-signal transducers based on EGOFET architectures.

MATERIALS AND METHODS

Source and Drain Patterning

Drawings of the source and drain electrodes by computer-aided design (CAD) were uploaded in the control software of a laser scan marker (ScribaR, ScribaNanotecnologie Srl, Bologna, Italy). The pattern was transferred onto a quartz slide (Phasis, Geneva, Switzerland) coated with a thin film of Au (50 nm thick) with a Ti (2 nm thick) adhesive layer. The scan marker featured a short-pulsed Nd:YAG infrared (IR)-laser (center wavelength λ = 1064 nm) together with three inertial micrometric motors controlling both the focal distance z of the laser and the x-y displacement of the sample holder. The positioning accuracy in x and y was less than 1 μm. The interdigitated electrodes of the channel layout have a W/L ratio of 2100, a channel length of 12 μm, the channel area A_{ch} = 3.0 10^{-3} cm^2. Further information can be found elsewhere.[31]

Pentacene Thin-Film Growth

Pentacene thin films (of nominal thickness 15 nm, corresponding to 10 monolayers) were deposited by sublimation in a high vacuum chamber (base pressure < 10^{-7} mbar) from a Knudsen cell at a rate of 0.125 Å/s (≈ 0.5 monolayer/min). The nominal thickness is read from a calibrated quartz microbalance. The pentacene growth followed standard protocols.[32]

Device Characterization

An aqueous solution of NaH_2PO_4 and Na_2HPO_4 (1:1, 100 mM as final concentration) was used as electrolyte, the pH of which was systematically changed by the addition of small aliquots of concentrated HCl or NaOH. A Pt wire (800 μm diameter) immersed in the electrolyte acted as the gate electrode. The gate area A_G is 0.36 cm^2. A polypropylene pool sealed onto the active area of the electronic device by means of a thin layer of poly-di-methyl-siloxane served to confine the electrolyte solution. The electrical characterization of the EGOFET was performed using a Keithley 2602 source meter.

HMDS Functionalization

After being treated with air plasma (Pelco EasyGlow™ set to 30 mV) for 15 min, the devices were left overnight in a chamber saturated with HMDS vapors. Pentacene deposition on these samples followed the protocol already discussed.

ASSOCIATED CONTENT

Supporting Information

Transfer Characteristic in linear regime and Output characteristics; Overlay of the non-offset transfer characteristics at different pH values; AFM of the pentacene film in the transistor channel; pH-dependence of EGOFET devices built on 3-Amino-Propyl-Tri-Etoxy-Silane (APTES)-functionalized quartz; pH-dependence of the on/off ratio.

This material is available free of charge via the Internet at http://pubs.acs.org

AUTHOR INFORMATION

Corresponding Author

* fabio.biscarini@unimore.it

Author Contributions

The manuscript was written through contributions of all authors.

Funding Sources

This work was funded by the EU 7th Framework Programme [FP7/2007–2013] under Grant Agreement No. 280772, “Implantable Organic Nanoelectronics (I-ONE-FP7)” project. MG is funded by the Engineering and Physical Sciences Research Council (EP/N02673X/1) and the Università di Modena e Reggio Emilia for a Visiting Professorship.

REFERENCES

(1) Bergveld, P. The Operation of an ISFET as an Electronic Device. Sens. Actuators 1981, 1, 17–29.

(2) Bergveld, P. ISFET , Theory and Practice. IEEE Sens. Conf. Toronto 2003, No. October, 1–26.

(3) Bartic, C.; Palan, B.; Campitelli, A.; Borghs, G. Monitoring pH with Organic-Based Field-Effect Transistors. Sens.Actuators, B; 2002; Vol. 83, pp 115–122.

(4) Bartic, C.; Campitelli, a.; Borghs, S. Field-Effect Detection of Chemical Species with Hybrid Organic/inorganic Transistors. Appl. Phys. Lett. 2003, 82 (3), 475–477.

(5) Ritjareonwattu, S.; Yun, Y.; Pearson, C.; Petty, M. C. Enhanced Sensitivity of an Organic Field-Effect Transistor pH Sensor Using a Fatty Acid Langmuir–Blodgett Film. Org. Electron. 2010, 11 (11), 1792–1795.

(6) Ritjareonwattu, S.; Yun, Y.; Pearson, C.; Petty, M. C. An Ion Sensitive Organic Field-Effect Transistor Incorporating the Ionophore Valinomycin. IEEE Sens. J. 2012, 12 (5), 1181–1186.

(7) Park, Y. M.; Salleo, A. Dual-Gate Organic Thin Film Transistors as Chemical Sensors. Appl. Phys. Lett. 2009, 95 (13), 133307.

(8) Spijkman, M.-J.; Brondijk, J. J.; Geuns, T. C. T.; Smits, E. C. P.; Cramer, T.; Zerbetto, F.; Stoliar, P.; Biscarini, F.; Blom, P. W. M.; de Leeuw, D. M. Dual-Gate Organic Field-Effect Transistors as Potentiometric Sensors in Aqueous Solution. Adv. Funct. Mater. 2010, 20 (6), 898–905.

(9) Kergoat, L.; Herlogsson, L.; Braga, D.; Piro, B.; Pham, M.-C.; Crispin, X.; Berggren, M.; Horowitz, G. A Water-Gate Organic Field-Effect Transistor. Adv. Mater. 2010, 22 (23), 2565–2569.

(10) Cramer, T.; Campana, A.; Leonardi, F.; Casalini, S.; Kyndiah, A.; Murgia, M.; Biscarini, F. Water-Gated Organic Field Effect Transistors – Opportunities for Biochemical Sensing and Extracellular Signal Transduction. J. Mater. Chem. B 2013, 1 (31), 3728.

(11) Cramer, T.; Kyndiah, A.; Murgia, M.; Leonardi, F.; Casalini, S.; Biscarini, F. Double Layer Capacitance Measured by Organic Field Effect Transistor Operated in Water. Appl. Phys. Lett. 2012, 100 (14), 143302.

(12) Kofler, J.; Schmoltner, K.; Klug, A.; List-Kratochvil, E. J. W. Hydrogen Ion-Selective Electrolyte-Gated Organic Field-Effect Transistor for pH Sensing. Appl. Phys. Lett. 2014, 104.

(13) Buth, F.; Kumar, D.; Stutzmann, M.; Garrido, J. a. Electrolyte-Gated Organic Field-Effect Transistors for Sensing Applications. Appl. Phys. Lett. 2011, 98 (15), 153302.

(14) Buth, F.; Donner, A.; Sachsenhauser, M.; Stutzmann, M.; Garrido, J. A. Biofunctional Electrolyte-Gated Organic Field-Effect Transistors., Adv. Mater. 2012, 4511–4517.

(15) Casalini, S.; Leonardi, F.; Cramer, T.; Biscarini, F. Organic Field-Effect Transistor for Label-Free Dopamine Sensing. Org. Electron. 2013, 14 (1), 156–163.

(16) Kergoat, L.; Piro, B.; Berggren, M.; Pham, M.-C.; Yassar, A.; Horowitz, G. DNA Detection with a Water-Gated Organic Field-Effect Transistor. Org. Electron. 2012, 13 (1), 1–6.

(17) Casalini, S.; Dumitru, A. C.; Leonardi, F.; Bortolotti, C. A.; Herruzo, E. T.; Campana, A.; Oliveira, R. F. De; Cramer, T.; Garcia, R.; Biscarini, F. Multiscale Sensing of Antibody À Antigen Interactions by Organic Transistors and Single-Molecule Force Spectroscopy. ACS Nano 2015, 9 (5), 5051–5062.

(18) Campana, A.; Cramer, T.; Simon, D. T.; Berggren, M.; Biscarini, F. Electrocardiographic Recording with Conformable Organic Electrochemical Transistor Fabricated on Resorbable Bioscaffold. Adv. Mater. 2014, 26, 3874–3878.

(19) Magliulo, M.; Mallardi, A.; Gristina, R.; Ridi, F.; Sabbatini, L.; Cioffi, N.; Palazzo, G.; Torsi, L. Part per Trillion Label-Free Electronic Bioanalytical Detection. Anal. Chem. 2013, 85 (8), 3849–3857.

(20) Cramer, T.; Chelli, B.; Murgia, M.; Barbalinardo, M.; Bystrenova, E.; de Leeuw, D. M.; Biscarini, F. Organic Ultra-Thin Film Transistors with a Liquid Gate for Extracellular Stimulation and Recording of Electric Activity of Stem Cell-Derived Neuronal Networks. Phys. Chem. Chem. Phys. 2013, 15 (11), 3897.

(21) Yates, D.; Levine, S.; Healy, T. Site-Binding Model of the Electrical Double Layer at the Oxide/water Interface. J. Chem. Soc. 1974.

(22) Levy, A.; Andelman, D.; Orland, H. Dielectric Constant of Ionic Solutions: A Field-Theory Approach. Phys. Rev. Lett. 2012, 108 (June), 1–5.

(23) Dill, K. A.; Bromberg, S. Molecular Driving Forces: Statistical Thermodynamics in Chemistry and Biology; Garland Science, 2003.

(24) Kosmulski, M. The pH Dependent Surface Charging and Points of Zero Charge. VI. Update and New Approach. J. Colloid Interface Sci. 2009, 337 (2), 439–448.

(25) Iler, R. The Chemistry of Silica: Solubility, Polymerization, Colloid and Surface Properties, and Biochemistry; 1979.

(26) Van Hal, R. E. G.; Eijkel, J. C. T.; Bergveld, P. A General Model to Describe the Electrostatic Potential at Electrolyte Oxide Interfaces. Adv. Colloid Interface Sci. 1996, 69 (1-3), 31–62.

(27) Scales, P. J.; Grieser, F.; Healy, T. W.; White, L. R.; Chan, D. Y. C. Electrokinetics of the Silica-Solution Interface: A Flat Plate Streaming Potential Study. Langmuir 1992, 8 (March 1992), 965–974.

(28) Kakudate, T.; Yoshimoto, N.; Saito, Y. Polymorphism in Pentacene Thin Films on Si O 2 Substrate Polymorphism in Pentacene Thin Films on SiO 2 Substrate. Appl. Phys. Lett. 2007, 081903, 43–46.

(29) Li, N.; Ho, C.-M. Photolithographic Patterning of Organosilane Monolayer for Generating Large Area Two-Dimensional B Lymphocyte Arrays. Lab Chip 2008, 8 (12), 2105–2112.

(30) Palazzo, G.; Tullio, D. De; Magliulo, M.; Mallardi, A.; Intranuovo, F.; Mulla, M. Y.; Favia, P.; Vikholm-lundin, I.; Torsi, L. Detection Beyond Debye ' S Length with an Electrolyte-Gated Organic Field-Effect Transistor. Adv. Mater. 2015, *27*, 911–916.

(31) Campana, A.; Cramer, T.; Greco, P.; Foschi, G.; Murgia, M.; Biscarini, F. Facile Maskless Fabrication of Organic Field-Effect Transistors on Biodegradable Substrates Appl. Phys. Lett. 2013, 103 (7), 073302.

(32) Quiroga, S. D.; Shehu, A.; Albonetti, C.; Murgia, M.; Stoliar, P.; Borgatti, F.; Biscarini, F. A High-Vacuum Deposition System for in Situ and Real-Time Electrical Characterization of Organic Thin-Film Transistors. Rev. Sci. Instrum. 2011, 82 (2), 025110.

Table of Contents Graphic